TRANSMUTATION AND PHASE STABILITY OF TUNGSTEN ARMOR IN FUSION POWER PLANTS

G. A. COTTRELL,* R. PAMPIN, and N. P. TAYLOR
EURATOM/United Kingdom Atomic Energy Authority Fusion Association, Culham Science Centre
Abingdon, Oxfordshire OX14 3DB, United Kingdom

Received October 5, 2005
Accepted for Publication December 12, 2005

We present calculations of the transmutation of initially pure tungsten first-wall and divertor plasma-facing armor into W-Re-Os alloys in the European Union Power Plant Conceptual Study (PPCS) fusion plant models A, B, and AB. The fusion neutron spectrum was modeled using the MCNP Monte Carlo code including resonance self-shielding effects, and we have calculated the evolution of the W-Re-Os alloy compositions. Trajectories of the alloys in the thermodynamic phase diagram show that the alloys remain in the single body-centered-cubic phase for their service lifetimes. Results for PPCS models A and B with soft neutron spectra show that the first-wall armor transmutes to an end-of-service alloy composition of approximately 91 at.% tungsten, 6 at.% rhenium, and 3 at.% osmium at its rear face. On the plasma-facing side of the tungsten, the effect of neutron shielding is larger. For PPCS model AB, the neutron spectrum is energetically harder, resulting in significantly lower tungsten transmutation rates.

KEYWORDS: *tungsten, transmutation, plasma-facing armor*

I. INTRODUCTION

Current design studies of fusion power plants, for example, the European Union Power Plant Conceptual Study[1] (PPCS), are based on the divertor tokamak concept. Such power plant concepts resemble present-day machines but are larger and possess the additional structures of a tritium breeding blanket as well as an outer radiation shield. Inside the shield, the various structures will be exposed to fluxes of 14-MeV deuterium-tritium (D-T) fusion neutrons. Low-activation neutron-irradiation resistant steels are being developed for these components. The supporting structure itself will however also need to be protected from surface damage and erosion resulting from direct plasma exposure. In the case of ferritic steel structural components (e.g., EUROFER in the PPCS models considered here), it will also be important to protect the surface from direct contact with the hydrogenic fuel, thus avoiding gas permeation and possible subsequent hydrogen embrittlement during neutron irradiation.[2] Plasma-material interaction will occur both at the first wall and divertor plasma-facing surfaces. Protection will be given by interposing a layer of suitably chosen plasma-facing material (PFM) "armor" between the plasma and the structural components.

*E-mail: geoff.cottrell@ukaea.org.uk

II. TUNGSTEN ARMOR

Tungsten is generally considered to be the most promising choice for power plant PFM armor,[3] both in the divertor and at the first wall. The tungsten is assumed to have no structural function in either of these roles, although it will need to accommodate thermal stresses. Tungsten possesses a high melting point, has a high thermal conductivity, and has a relatively low thermal expansion. Because of its high cohesive energy, it has a high resistance against sputtering and erosion. For example, for ITER-like conditions, the erosion rate of tungsten [~0.1 mm/full-power year (FPY)] is much lower than low-Z materials such as beryllium (~3 mm/FPY). The disadvantages of tungsten are high values of the ductile-brittle transition temperature (DBTT), recrystallization temperature (RCT), and its hardness. There are only limited data available for these in neutron-irradiated tungsten. For irradiated tungsten alloys the presently known temperature window range extends from 800 to 1200°C, defined by the DBTT at the lower end and by the RCT at the upper end of the range.

In the PPCS study, the divertor lifetime was maximized by choosing a tungsten alloy divertor target PFM; the long service life results from tungsten's low sputtering yield for low-energy plasma particles. The tritium retention rates on tungsten surfaces are expected to be low.

Under steady-state conditions, the divertor is expected to be able to handle a maximum peak power flux of 15 MW m^{-2}, and the PPCS models assume that the divertor will be operated in such a way as to mitigate any transient power loads on the material surfaces. The blanket modules are assumed to be faced with a 2-mm-thick layer of tungsten armor. An overview of the expected physical conditions and required properties of the PFM materials is given in Table I.

With tungsten as the PPCS primary armor material choice,[2] it is appropriate to investigate any possible changes to its mechanical properties and composition that result from its interaction with fusion neutrons and determine its evolution in a power plant. An important property of tungsten is its high rate of transmutation to rhenium and osmium in a fusion neutron environment.[4,5] To assess this effect in the PPCS models, we have assumed initially pure tungsten with natural isotopic abundances.

Natural tungsten is made of five stable isotopes: ^{180}W (0.13%), ^{182}W (26.3%), ^{183}W (14.3%), ^{184}W (30.7%), and ^{186}W (28.6%). Under typical fusion neutron spectra, the bulk of the transmutation products arises from (n,γ) and $(n,2n)$ reactions and leads mainly to rhenium and osmium isotopes. The principal pathways for their generation are

$$^{186}\mathrm{W}(n,\gamma)^{187}\mathrm{W}$$

$$\rightarrow (\beta-)\ ^{187}\mathrm{Re}\begin{cases}(n,\gamma)^{188m}\mathrm{Re}\rightarrow(\gamma)\ ^{188}\mathrm{Re}\rightarrow(\beta)\ ^{188}\mathrm{Os}\\(n,2n)^{186}\mathrm{Re}\rightarrow(\beta-)\ ^{186}\mathrm{Os}\end{cases}$$

$$^{184}\mathrm{W}(n,\gamma)^{185}\mathrm{W}\rightarrow(\beta-)\ ^{185}\mathrm{Re}(n,\gamma)^{186}\mathrm{Re}\rightarrow(\beta-)\ ^{186}\mathrm{Os}\ .$$

Neutron absorption in ^{180}W generates traces of tantalum through β^+ decay of ^{181}W. The relative importance of these pathways is strongly dependent on the neutron spectra and therefore on the surrounding materials. The $^{186}\mathrm{W}(n,\gamma)^{187}\mathrm{W}$ reaction cross section is shown in Fig. 1. It follows a typical inverse projectile velocity law at low energies followed by a region of fine, individual resonances. At an energy of ~20 eV, there is a giant capture resonance with a peak cross-section value of ~20 000 b. The neutron flux in this spectral region typically shows a local depression at the resonance edge, where the absorption channel is dominant. This behavior can introduce a systematic overestimation of the transmutation rates of tungsten in fusion environments unless adequate geometry and energy treatments are used.[6,7] The effect is called self-shielding and was included in the calculations presented here.

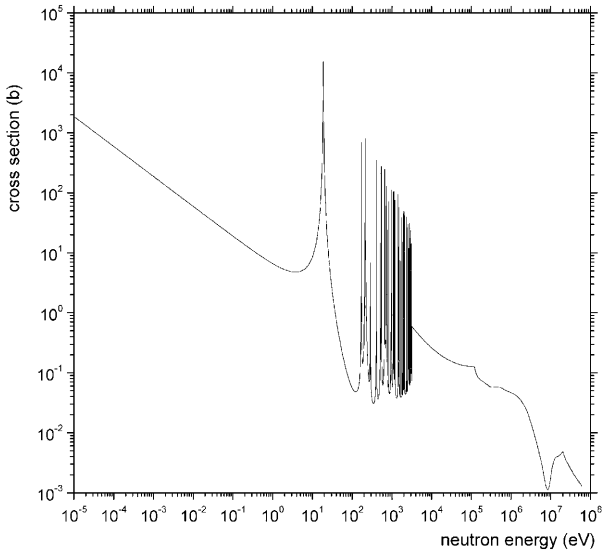

Fig. 1. Cross section for the $^{186}\mathrm{W}(n,\gamma)^{187}\mathrm{W}$ reaction (in units of barns).

III. MODELING THE PPCS NEUTRON SPECTRA

The PPCS power plants studied were models A, B, and AB (Refs. 1 and 8). All three are based on relatively conservative extrapolations of present-day plasma performance, but they differ from each other in the

TABLE I

Physical Conditions and General Requirements of Tungsten Plasma-Facing Armor Assumed in the PPCS Fusion Power Plants

	First Wall	Divertor
Operating temperature (K)	~750	<1500
Mean thermal load (MW m^{-2})	<0.5	<15
Mean neutron load (MW m^{-2})	2 to 2.2	~1
Flux of hydrogenic charge-exchange atoms striking surface ($m^{-2}\,s^{-1}$)	$<10^{18}$	$<10^{24}$
Mean energies of these atoms (eV)	<10 000	<5
Plasma quiescence	Some plasma-material interaction assumed	Steady state
Service lifetime required (yr)	5	2.5

following respects. Model A is based on pressurized water reactor–like technology with a water-cooled divertor and blanket and LiPb tritium breeder. Models B and AB are both based on higher blanket outlet temperatures (utilizing helium gas cooling) giving higher thermal efficiencies. Model B is characterized by a pebble bed breeding blanket (with a beryllium neutron multiplier), which is where it differs from model AB, which again is based on a LiPb breeder and multiplier technology with no beryllium present. A summary of the relevant parameters is given in Table II.

For accurate modeling of the neutron transport and calculation of the neutron spectra in the PPCS models, detailed geometrical models were used in the Monte Carlo calculations. These calculations were performed on a parallel computer cluster of 72 dual processors that, together with the use of variance reduction techniques, greatly improved the efficiency of the calculations and minimized the statistical errors of the Monte Carlo results. Figures 2 and 3 show the geometries of the first wall and divertor, respectively, with enlarged views in the vicinity of the tungsten-armored components. For each PPCS design, details of the materials within the different structures are given in Table III.

The neutron spectra averaged within the volume of the first wall tungsten armor in the three PPCS models are shown in Fig. 4. In each case the large peak at a neutron energy of 14 MeV corresponds to the birth energy of the D-T neutrons in the plasma. Lower-energy neutrons result from multiple collisions that occur in the blanket and outer structures. Differences between the spectra of PPCS models A and B appear to be largely due to the different amounts of moderation in the water and

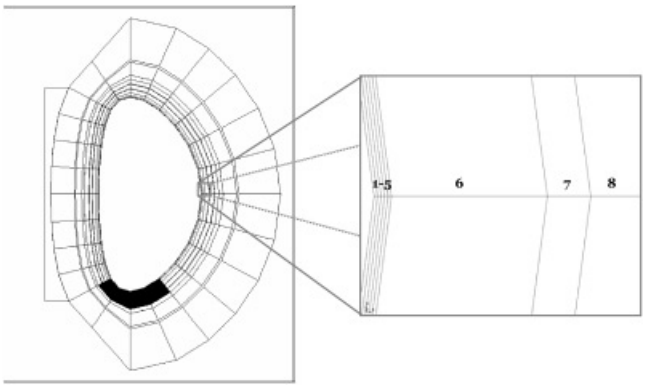

Fig. 2. PPCS model showing detail of first wall/blanket structure.

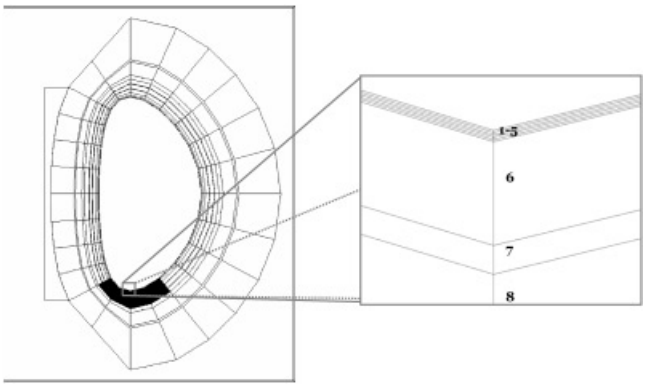

Fig. 3. PPCS model showing detail of divertor structure.

TABLE II

Summary of PPCS Main Features and Materials

	Model A	Model B	Model AB
Fusion power (GW)	5	3.6	4.29
Major radius (m)	9.55	8.6	9.56
Average neutron wall load (MW m^{-2})	2.2	2.0	1.8
Divertor peak heat load (MW m^{-2})	15	10	10
Blanket			
Structural material	EUROFER	EUROFER	EUROFER
Coolant/T_{outlet} (°C)	H_2O/325	Helium/500	Helium/500
Breeder/neutron multiplier	LiPb/LiPb	Li_4SiO_4 pebble bed/beryllium	LiPb/LiPb
Divertor			
Structural material	[CuCrZr alloy]	Tungsten alloy	Tungsten alloy
Armor material	Tungsten alloy	Tungsten alloy	Tungsten alloy
Coolant	H_2O	Helium	Helium

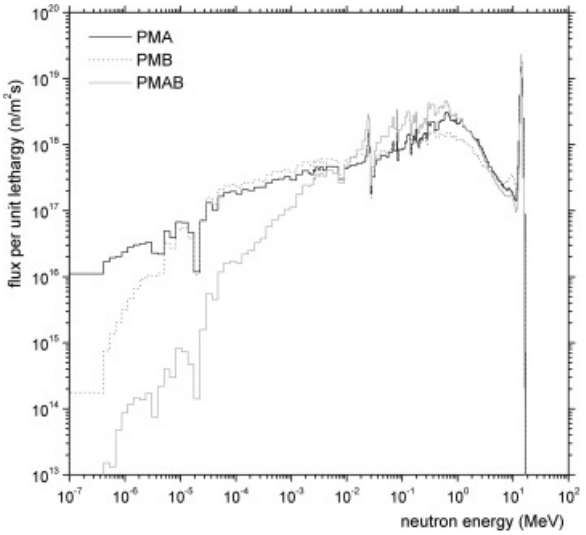

Fig. 4. Neutron spectra averaged within the volume of the first-wall tungsten armor in the three PPCS models.

beryllium. These differences are, however, small compared with the case of model AB where, for neutron energies below ~1 keV, the neutron flux is up to approximately 100 times smaller. This harder spectrum results from the lack of strongly moderating materials (model AB is unique in that it is based on helium gas cooling throughout and there is no beryllium neutron multiplier/moderator in the blanket).

The spectra in Fig. 4 also show the narrow resonance absorption dip at a narrow band of neutron energies of ~20 eV, illustrating the effect of the tungsten self-shielding. To investigate this effect further, in our numerical model, we divided the 2-mm-thick tungsten into discrete regions. In each of these we have calculated the effective transmutation cross section:

$$\sigma_{eff} = \frac{RR_{MCNP}}{N_W \phi_{MCNP}} ,$$

where

RR_{MCNP}, ϕ_{MCNP} = transmutation rate for the $^{186}W(n,\gamma)^{187}W$ reaction and total neutron flux, respectively, both calculated using the MCNP code using a continuous energy representation and integrated over all neutron energies and over the volume of the region

N_W = density of tungsten target atoms in the armor.

TABLE III

Details of the Materials Composition and Structure of the First Wall and Divertor Armor Models of Figs. 2 and 3

Region	Plant Model	Layer Number	Thickness (mm)	Component	Material Composition
First wall	PMA	1 through 5	0.4	Armor	Tungsten
		6	10	First wall	EUROFER + water
		7	11	First wall	EUROFER
		8	~850	Breeder zone	EUROFER + $Li_{17}Pb_{83}$ + water
	PMB	1 through 5	0.4	Armor	Tungsten
		6	18	First wall	EUROFER + helium
		7	5	First wall	EUROFER
		8	~500	Breeder zone	EUROFER + Be + Li_4SiO_4 + helium
	PM-AB	1 through 5	0.4	Armor	Tungsten
		6	15	First wall	EUROFER + helium
		7	10	First wall	EUROFER + helium
		8	~700	Breeder zone	EUROFER + $Li_{17}Pb_{83}$ + helium
Divertor	PMA	1 through 5	0.4	Plates	Tungsten
		6	10	Heat sink	EUROFER + tungsten + CuCrZr + OFHCu + water
		7	11	Heat sink	
		8	~850	Structure	EUROFER + water
	PMB	1 through 5	0.4	Plates	Tungsten
		6	18	Heat sink	EUROFER + tungsten + helium
		7	5	Heat sink	
		8	~500	Structure	EUROFER + helium
	PM-AB	1 through 5	0.4	Plates	Tungsten
		6	15	Heat sink	EUROFER + tungsten + helium
		7	10	Heat sink	
		8	~700	Structure	EUROFER + helium

The resulting variation of σ_{eff} within the first-wall armor is shown in Fig. 5 for the three power plant models. Figure 5 shows neutron resonance self-shielding: For models A and B, the effective transmutation cross section drops from a value of ~1.2 to ~0.3 b (roughly one e-folding) in a distance of ~0.6 mm, measured from the rear face of the armor. This length scale is consistent with an order-of-magnitude estimate of the mean free path of a neutron having energy close to the peak of the giant resonance shown in Fig. 1 where the typical transmutation cross section is $\sigma_{res} \sim 1000$ b. There, the neutron mean free path is $(N_W \sigma_{res})^{-1} \sim 0.56$ mm. For the harder spectrum PPCS model AB, neutron shielding also takes place, but owing to the much smaller flux of neutrons at the resonant capture energies, the transmutation rates are smaller.

Figure 5 shows that σ_{eff} rises sharply at the rear face of the tungsten armor, in the region where the neutron self-shielding is smallest. Physically, this arises from the fact that the 2-mm-thick armor is almost transparent to the primary D-T 14-MeV fusion neutrons, which enter the blanket from the plasma side, passing through the tungsten with negligible transmutation rates, owing to their high energies. However, the rear face of the tungsten armor is exposed to the largest flux of moderated neutrons diffusing out of the blanket with energies close to the resonance peak. It is this moderated neutron flux that gives rise to the larger transmutation rate on the blanket-facing (rear) side of the tungsten armor. The first-wall neutron spectra at the front and rear faces of the first-wall armor for PPCS model A are shown in Fig. 6. The narrow spectral effect of the resonant self-shielding can again be seen in this case.

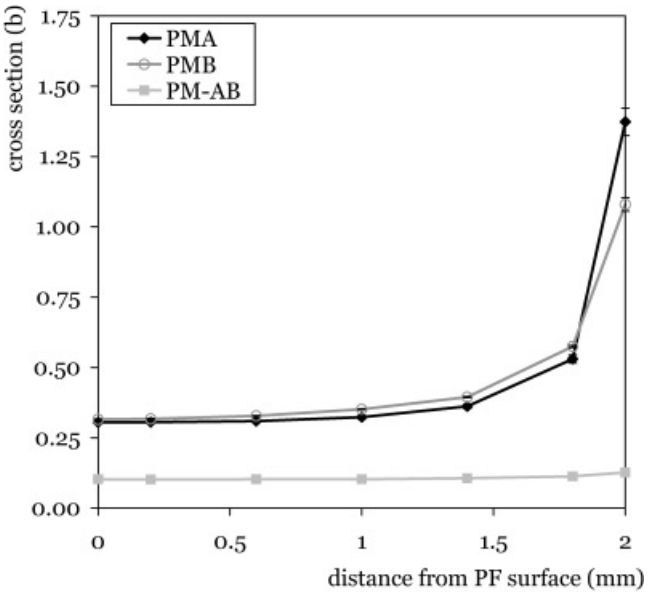

Fig. 5. Variation of effective cross section σ_{eff} within the 2-mm-thick first-wall armor for the three power plant models.

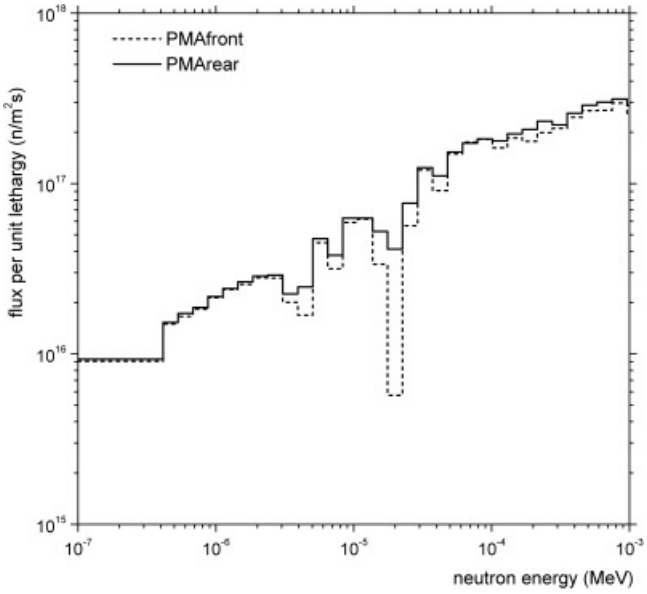

Fig. 6. Detailed neutron spectra for the front and rear faces of the first-wall 2-mm-thick tungsten armor in PPCS model A showing the effect of the self-shielding.

Figures 7a and 7b show the variation of σ_{eff} within the divertor tungsten-faced armor tiles for the three power plant models considered. Again, the resonant self-shielding is smallest at the rear face of the armor. The effect is most significant for PPCS model A; this is because this divertor design is the only one of the three considered that uses water cooling. The water, lying behind the tiles, strongly moderates the local neutron spectrum and enhances the transmutation rate. In models B and AB, the divertor tiles are cooled by helium gas; the effect of the reduced local neutron moderation in these models is reflected in the reduced values of σ_{eff}.

The overestimation of the reaction rate due to a multigroup numerical treatment was investigated by comparing the σ_{eff} values obtained with the continuous energy treatment and those calculated by the FISPACT code using 175-energy-group data: a factor of up to 4 was found for the lower-moderation case of plant model AB. In general, the more similar the neutron spectra are to the functions used in the weighting of the multigroup data, the closer the two effective cross-section values are: The difference is significantly smaller for the moderated spectra at the rear interface of the armor with the blanket of plant models A and B (Ref. 9).

IV. TUNGSTEN TRANSMUTATION RESULTS

Transmutation calculations were made using the neutron spectra described above. The cross-section data were obtained from the most recent versions of the FISPACT

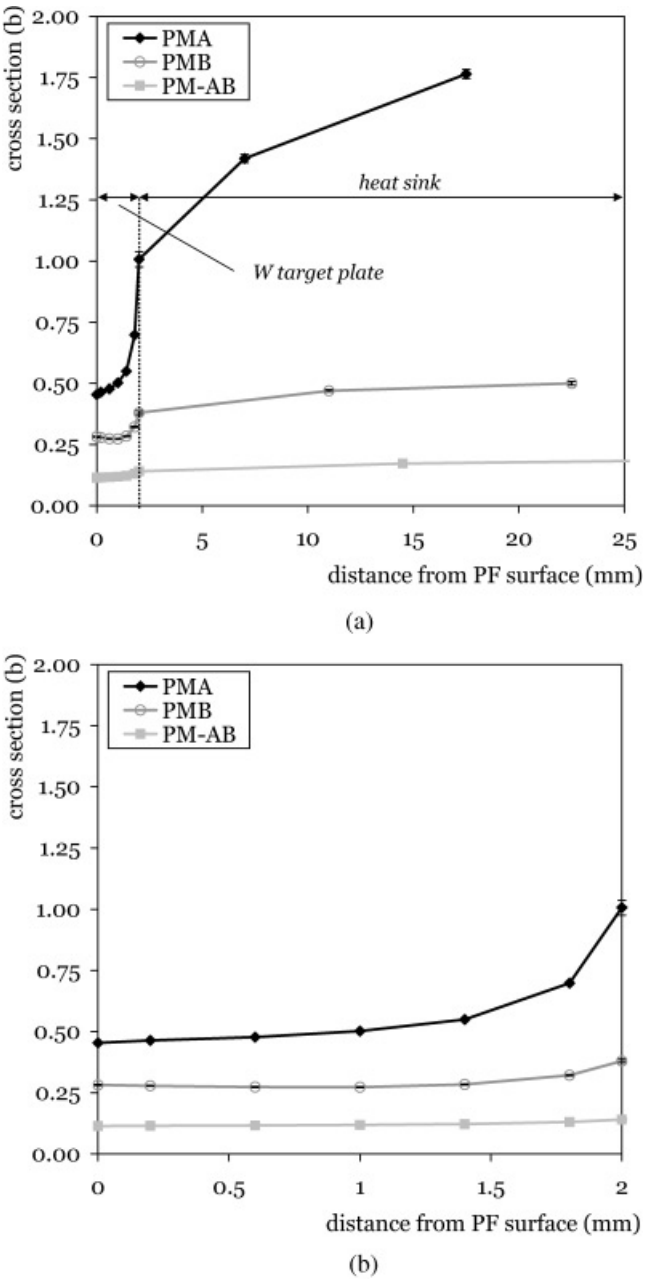

Fig. 7. (a) Variation of effective cross section σ_{eff} within assumed 25-mm-thick divertor armor tiles for the three power plant models. (b) Enlarged detail of the variation of effective cross section σ_{eff} within the 2-mm-thick tungsten divertor armor tile facing for the three power plant models.

2003 and EAF discrete data libraries.[10] Appropriate commands were used in order to override the $^{186}W(n,\gamma)^{187}W$ reaction rates calculated by FISPACT using multigroup data and to replace these with those obtained in the neutron transport calculations using continuous energy treatment with MCNP, described above. Irradiation histories of pure tungsten material were followed for 10 yr of continuous irradiation, encompassing the required power plant service lifetimes given in Table I.

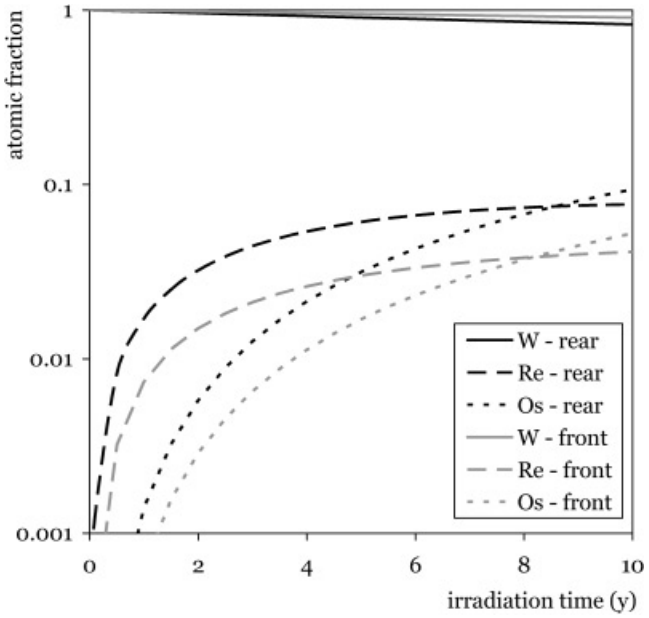

Fig. 8. Temporal evolution of the tungsten-rhenium-osmium atomic fractional alloy composition for the first-wall armor in model A, divided into front (i.e., plasma-facing) and rear (blanket-facing) faces.

Figure 8 shows the temporal evolution of the tungsten-rhenium-osmium alloy composition for the first wall armor in model A, divided into front (plasma-facing) and rear (blanket-facing) regions of interest. The effect of neutron self-shielding on the alloy composition evolution is clear: The rear face of the armor develops significantly higher rhenium and osmium concentrations in the 5-yr service life than the front. The alloy compositions for this and the other first-wall models are given in Table IV. These results can be compared with the temporal evolution of the

TABLE IV

Compositions of the Tungsten-Rhenium-Osmium First-Wall Alloys After the Assumed Service Lifetime of 5 yr in the PPCS Models*

Element	Tungsten		Rhenium		Osmium	
Face	Rear	Front	Rear	Front	Rear	Front
PPCS model A	90.8	95.3	6.1	3.0	3.2	1.7
PPCS model B	91.0	94.5	5.6	3.5	3.3	1.9
PPCS model AB	97.1	97.2	2.7	2.6	0.3	0.2

*Units: atomic percent.

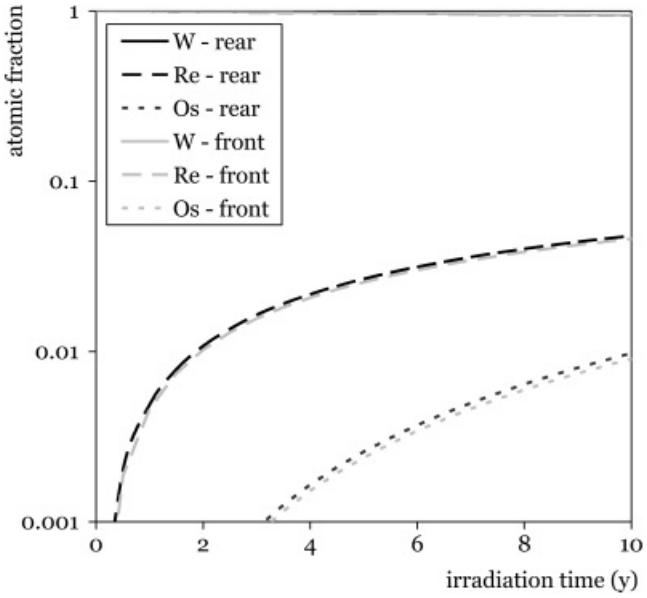

Fig. 9. Temporal evolution of the tungsten-rhenium-osmium alloy atomic fractional composition for the first-wall armor in model AB.

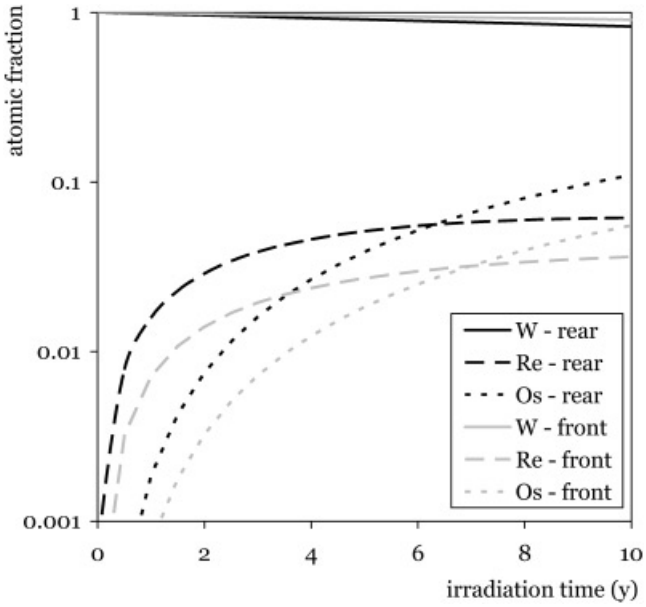

Fig. 10. Temporal evolution of the tungsten-rhenium-osmium alloy atomic fractional composition in the divertor tungsten for model A.

tungsten-rhenium-osmium alloy composition for the first-wall armor in model AB (Fig. 9). Overall, the transmutation rate in this model is lower than in either model A or B, a consequence of the harder neutron spectrum in model AB. The alloy compositions also show less front-/rear-face difference, resulting from of the absence of nearby moderating materials behind the armor.

Results for the evolution of the tungsten-rhenium-osmium alloy composition in the divertor tungsten are shown in Fig. 10 (model A) and in Fig. 11 (model AB). Alloy compositions are given in Table V. The larger difference between the front/rear compositions of model A compared with either model B or AB is due to the moderating effect of the water coolant in model A.

TABLE V

Compositions of the Tungsten-Rhenium-Osmium Divertor Alloys After the Assumed Service Lifetime of 2.5 yr in the PPCS Models*

Element	Tungsten		Rhenium		Osmium	
Face	Rear	Front	Rear	Front	Rear	Front
PPCS model A	95.4	97.8	3.4	1.7	1.2	0.5
PPCS model B	97.6	97.9	2.1	1.8	0.4	0.4
PPCS model AB	98.6	98.8	1.3	1.1	0.1	0.06

*Units: atomic percent.

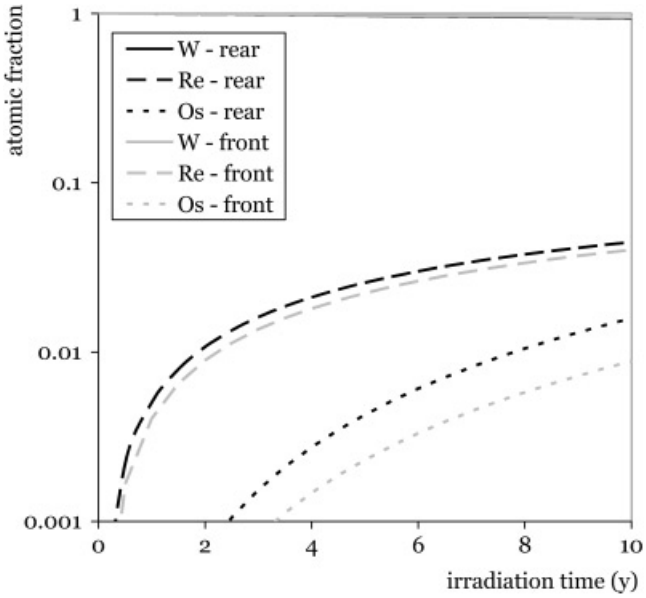

Fig. 11. Temporal evolution of the tungsten-rhenium-osmium alloy atomic fractional composition in the divertor tungsten for model AB.

V. TRAJECTORIES IN THE THERMODYNAMIC PHASE DIAGRAM

Pure tungsten exists naturally in the α, or body-centered-cubic (bcc), structure, but when alloyed with

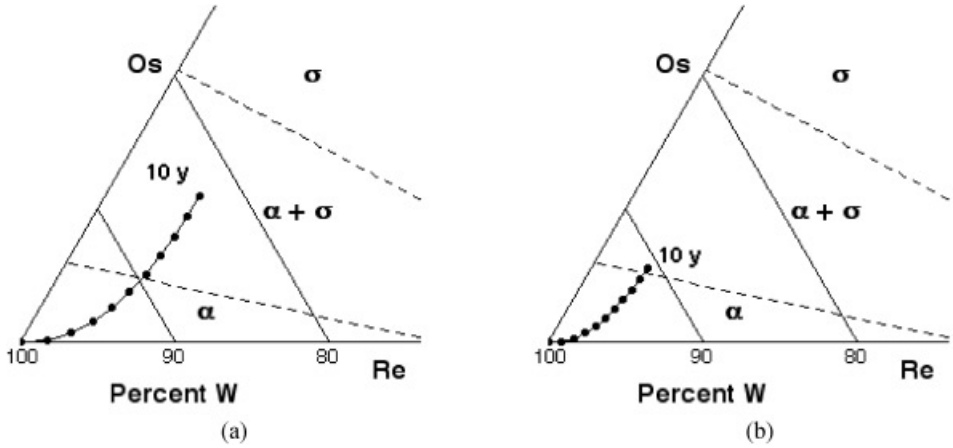

Fig. 12. Ternary phase diagrams for the tungsten-rhenium-osmium alloy system showing trajectories of composition change due to neutron irradiation of the (a) rear (blanket)-facing and (b) front (plasma)-facing tungsten in PPCS model A first wall. The points indicated mark the times, in years, at which the points on this path are reached. The ternary field boundaries are interpolated from the binary phase equilibria at 1500°C.

rhenium and osmium, intermetallic compounds with undesirable mechanical properties can form. It is therefore important to analyze the stability of the tungsten-rhenium-osmium alloys expected in the ternary thermodynamic phase diagram as it is possible that alloy compositions could enter the extremely brittle pure σ or duplex $\alpha + \sigma$ phases. The binary phase diagrams[11] show that the $\alpha/(\alpha + \sigma)$ boundary at 1500°C occurs at ~94% tungsten, for tungsten-osmium, and at ~72% tungsten for tungsten-rhenium. Similarly, the $(\alpha + \sigma)/\sigma$ boundary occurs at ~79% tungsten (tungsten-osmium) and 56% tungsten (tungsten-rhenium).

Figure 12 shows trajectories of the PPCS first-wall alloys in the tungsten-rhenium-osmium ternary phase diagram. After one service life of 5 yr, the rear face of the first-wall tungsten armor approaches, but does not cross, the boundary separating the pure bcc α field from the duplex $\alpha + \sigma$ one. At the plasma-facing side of the armor, the material remains well within the pure bcc α field. The first-wall armor for all three PPCS models studied here remains inside the pure bcc α field for the service life of 5 yr.

Figure 13 shows the trajectories of the divertor tungsten-rhenium-osmium alloys in the phase diagram. After one service life of 2.5 yr, the rear face of the tungsten armor lies well within the pure bcc α field. The same

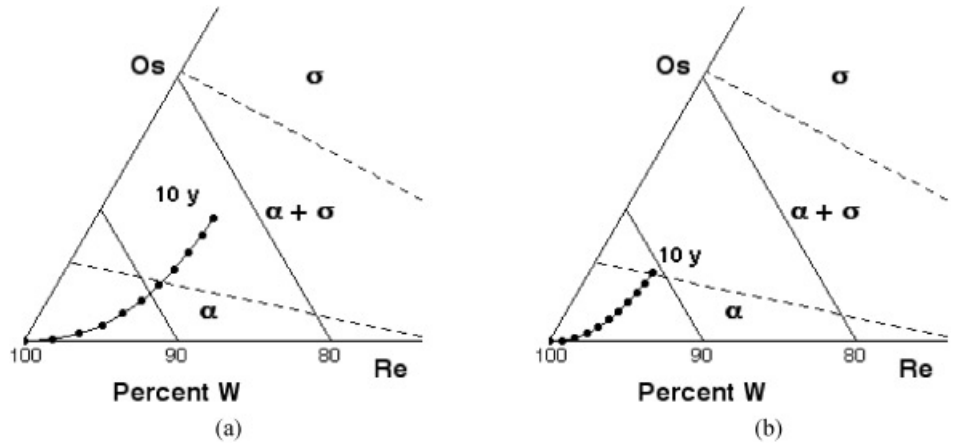

Fig. 13. Ternary phase diagrams for the tungsten-rhenium-osmium alloy system showing trajectories of composition change due to neutron irradiation of the (a) rear-facing and (b) front (plasma)-facing tungsten in PPCS model A divertor. The points indicated mark the times, in years, at which the points on this path are reached. The ternary field boundaries are interpolated from the binary phase equilibria at 1500°C.

is true for the front plasma-facing side. Thus, the divertor armor for all three PPCS models studied here remains inside the pure bcc α field for the service life of 2.5 yr.

VI. DISCUSSION AND CONCLUSIONS

The present study has examined the transmutation and thermodynamic phase stability of initially pure tungsten plasma-facing armor in three PPCS fusion power plant designs. The tungsten transforms into tungsten-rhenium-osmium alloys that, within the appropriate service lifetimes for the first-wall and divertor armor, remain inside the bcc α field and do not cross into the duplex $\alpha + \sigma$ or the pure σ fields where the material is likely to form brittle intermetallic compounds. In the present study we have included the effect of the resonant neutron self-shielding of tungsten, which has reduced the effective transmutation rate compared with earlier work[12] and has emphasized the importance of details of the power plant design, particularly with regard to the effect of the presence of neutron-moderating materials. The self-shielding results show that the transmutation rate of the armor is relatively large in a layer $\sim$0.5 mm thick facing the blanket for PPCS designs A and B, where appreciable neutron moderation takes place. In the alternative model AB design, using exclusively helium gas coolant and with no beryllium neutron multiplier in the blanket, the neutron spectrum is harder. The reduced flux of low-energy neutrons in this design results in a significantly lower transmutation rate.

Although the tungsten armor does not cross into the duplex $\alpha + \sigma$ or the pure σ fields of the phase diagram, the end-of-life concentrations of the solid transmutants rhenium and osmium are appreciable. For model A's first-wall armor, the end-of-life alloy composition is approximately 91 at.% tungsten, 6 at.% rhenium, and 3 at.% osmium, in the rear face of the material. The values for the model B first wall are similar. Thermodynamically, these impurities ought to form stable substitutional solid solutions in the tungsten. However, previous studies[13,14] of neutron-irradiated tungsten-rhenium alloys, with rhenium concentrations as low as 5%, indicate the formation of tungsten-rhenium and W-3Re platelet-like precipitates, indicating a nonequilibrium neutron-induced precipitation mechanism. These precipitates contribute to the hardening (increase in tensile stress) and also to an increase in the DBTT. Both of these mechanical property changes have been observed experimentally.[15,16] In their work on neutron-irradiated tungsten-rhenium alloys, Nemoto et al.[17] have expressed concerns regarding changes to the mechanical properties, in particular to the irradiation-induced hardening and embrittlement and the formation of σ-phase and χ-phase precipitates.[18]

There is a lack of data on the properties of neutron-irradiated tungsten alloys in the composition ranges relevant to the present study. However, if the tungsten-rhenium-osmium alloys discussed in this paper do undergo neutron-induced precipitation and thus suffer embrittlement, then this may be of concern, particularly as the largest transmutation rates in the first-wall armor occur at the rear, blanket-facing surface of the material where the armor will be bonded to a substrate. We believe that further neutron irradiation experimental work could usefully be done on tungsten-rhenium-osmium alloys, with compositions corresponding to different ages in fusion power plants. Obtaining such data will clarify the changes in mechanical properties and help to determine realistic service lifetimes for the tungsten armor components in a fusion power plant. To avoid the hardening and embrittling effects of any neutron-induced precipitates, possible alternatives could include the use of isotopically tailored tungsten in power plants or confining the use of natural tungsten to helium gas-cooled plants, like model AB, where the transmutation rates are significantly smaller.

ACKNOWLEDGMENTS

We thank I. Cook for encouragement and stimulating discussions. This work was funded jointly by the U.K. Engineering and Physical Sciences Research Council and by the European Community under the contract of Association between EURATOM and United Kingdom Atomic Energy Authority. The views and opinions expressed herein do not necessarily reflect those of the European Commission.

REFERENCES

1. D. MAISONNIER et al., "A Conceptual Study of Commercial Fusion Power Plants: Final Report of the European Power Plant Conceptual Study," EFDA-RP-RE-5.0, European Fusion Development Agreement Report (2004).

2. V. BARABASH et al., "Material/Plasma Surface Interaction Issues Following Neutron Damage," *J. Nucl. Mater.*, **313–316**, 42 (2003).

3. H. BOLT et al., "Materials for the PFCs of Fusion Reactors," *J. Nucl. Mater.*, **329–333**, 66 (2004).

4. L. R. GREENWOOD and F. A. GARNER, "Transmutation of Mo, Re, W, Hf and V in Various Irradiation Test Facilities," *J. Nucl. Mater.*, **212–215**, 635 (1994).

5. C. B. A. FORTY et al., "Burnup of Some Refactory Metals in a Fusion Neutron Spectrum," *J. Nucl. Mater.*, **212–215**, 640 (1994).

6. M. E. SAWAN, H. KHATER, H. IIDA, and R. T. SANTORO, "Self-Shielding Effects in Decay Heat Calculations for Tungsten," *Fusion Technol.*, **34** 1008 (1998).

7. J.-CH. SUBLET and M. E. SAWAN, "Self-Shielding Effects in a W Layer in a Fusion Device," *Fus. Eng. Des.*, **45**, 65 (1999).

8. A. Li PUMA et al., "Breeding Blanket Design and Systems Integration for a Helium-Cooled Lithium-Lead Fusion Power Plant," *Fusion Eng. Des.*, **81**, *1–7*, 469 (Feb. 2006).

9. R. PAMPIN, "Tungsten Transmutation and Resonance Self-Shielding in PPCS Models for the Study of Sigma-Phase Formation," UKAEA FUS 525, United Kingdom Atomic Energy Authority (2005).

10. R. A. FORREST, "FISPACT-2003: User Manual," AEA FUS 485, United Kingdom Atomic Energy Authority (2003).

11. *Binary Alloy Phase Diagrams*, 2nd ed., T. B. MASSALSKI, Ed., ASM International (1990).

12. G. A. COTTRELL, "Sigma Phase Formation in Irradiated Tungsten, Ta and Mo in a Fusion Power Plant," *J. Nucl. Mater.*, **334**, 166 (2004).

13. R. K. WILLIAMS et al., "Irradiation Induced Precipitation in W Based W-Re Alloys," *Metall. Trans A.*, **14A**, 655 (1983).

14. R. HERSCHITZ and D. N. SEIDMAN, "Radiation-Induced Precipitation in Fast Neutron Irradiated W-Re Alloys: An Atom Probe Field Ion Microscope Study," *Nucl. Instrum. Methods Phys. Res. B*, **7/8**, 137 (1985).

15. I. V. GORYNIN et al., "Effects of Neutron Irradiation on Properties of Refactory Metals," *J. Nucl. Mater.*, **191–194**, 421 (1992).

16. P. KRAUTWASSER et al., "Influence of Fast Neutron Fluence on the DBTT of W, W10Re and W3.4Ni1.6Fe," *Refactory Metals*, **77**, 673 (1989).

17. Y. NEMOTO et al., "Microstructural Development of Neutron Irradiated W-Re Alloys," *J. Nucl. Mater.*, **283–287**, 1147 (2000).

18. Y. NEMOTO et al., "Microstructural Development and Radiation Hardening of Neutron Irradiated Mo-Re Alloys," *J. Nucl. Mater.*, **324**, 62 (2004).